

**Original citation:**

Cho, K.-S., Bong, S.-C., Nakariakov, V. M., Lim, E.-K., Park, Y.-D., Chae, J. C., Yang, H.-S., Park, H.-M. and Yurchyshyn, V.. (2015) Intensity and Doppler velocity oscillations in pore atmospheres. *The Astrophysical Journal*, 802 (1). 45.

**Permanent WRAP URL:**

<http://wrap.warwick.ac.uk/78682>

**Copyright and reuse:**

The Warwick Research Archive Portal (WRAP) makes this work by researchers of the University of Warwick available open access under the following conditions. Copyright © and all moral rights to the version of the paper presented here belong to the individual author(s) and/or other copyright owners. To the extent reasonable and practicable the material made available in WRAP has been checked for eligibility before being made available.

Copies of full items can be used for personal research or study, educational, or not-for-profit purposes without prior permission or charge. Provided that the authors, title and full bibliographic details are credited, a hyperlink and/or URL is given for the original metadata page and the content is not changed in any way.

**Publisher's statement:**

Reproduced by permission of the AAS.

Published version: <http://dx.doi.org/10.1088/0004-637X/802/1/45>

**A note on versions:**

The version presented here may differ from the published version or, version of record, if you wish to cite this item you are advised to consult the publisher's version. Please see the 'permanent WRAP URL' above for details on accessing the published version and note that access may require a subscription.

For more information, please contact the WRAP Team at: [wrap@warwick.ac.uk](mailto:wrap@warwick.ac.uk)

# INTENSITY AND DOPPLER VELOCITY OSCILLATIONS IN PORE ATMOSPHERE

K.-S. CHO<sup>1,2</sup>, S.-C. BONG<sup>1</sup>, V. M. NAKARIAKOV<sup>3,4,5</sup>, E.-K. LIM<sup>1</sup>, Y.-D. PARK<sup>1</sup>, J. C. CHAE<sup>6</sup>, H.-S. YANG<sup>6</sup>, H.-M. PARK<sup>6</sup>, AND V. YURCHYSHYN<sup>1,7</sup>

## ABSTRACT

We have investigated chromospheric traveling features running across two merged pores from their centers at the speed about  $55 \text{ km s}^{-1}$ , in the active region AR 11828. The pores were observed on 2013 August 24 by using high time, spatial, and spectral resolution data from the Fast Imaging Solar Spectrograph (FISS) of the 1.6 meter New Solar Telescope (NST). We infer a LOS velocity by applying the lambdameter method to the Ca II 8542 Å band and H $\alpha$  band, and investigate intensity and the line-of-sight velocity changes at different wavelengths and different positions at the pores. We find that they have 3 minutes oscillations, and the intensity oscillation from the line center (0.0 Å) is preceded by that from the core (-0.3 Å) of the bands. There is no phase difference between the intensity and the LOS velocity oscillations at a given wavelength. The amplitude of LOS velocity from the near core spectra ( $\Delta\lambda = 0.10 - 0.21\text{Å}$ ) is greater than that from the far core spectra ( $\Delta\lambda = 0.24 - 0.36\text{Å}$ ). These results support the interpretation of the observed wave as a slow magnetoacoustic wave propagating along the magnetic field lines in the pores. The apparent horizontal motion and a sudden decrease of its speed beyond the pores can be explained by the projection effect caused by inclination of the magnetic field with a canopy structure. We conclude that the observed wave properties of the pores are quite similar to those from the sunspot observations.

---

<sup>1</sup>Korea Astronomy and Space Science Institute, Daejeon 305-348, Korea (kscho@kasi.re.kr)

<sup>2</sup>University of Science and Technology, Daejeon 305-348, Korea

<sup>3</sup>Physics Department, University of Warwick, Coventry CV4 7AL, UK

<sup>4</sup>School of Space Research, Kyung Hee University, Yongin, 446-701, Gyeonggi, Korea

<sup>5</sup>Central Astronomical Observatory of the Russian Academy of Sciences at Pulkovo, 196140 St Petersburg, Russia

<sup>6</sup>Astronomy Program, Department of Physics and Astronomy, Seoul National University, Seoul 151-747, Korea

<sup>7</sup>Big Bear Solar Observatory, New Jersey Institute of Technology, Big Bear City, CA 92314, USA

*Subject headings:* Sun: Pores – Sun: Oscillations – Sun: Magnetoacoustic waves

## 1. INTRODUCTION

Sunspot oscillations have been studied since their first discovery by Beckers & Tallant (1969). In particular, an excellent dataset of the oscillations has been presented by Rouppe van der Voort et al. (2003), and their Doppler signatures were studied by Tziotziou et al. (2006) and their thermal and magnetic properties were investigated by de la Cruz Rodrí et al. (2013). Three types of oscillations have been reported: the running penumbra waves (Zirin & Sterin 1972), five-minute oscillations in the umbra photosphere (Bhatnagar, Livingston, & Harvey 1972), and three-minute oscillations of umbra velocity and intensity in the chromosphere (Giovanelli 1972). The three-minute oscillations are manifested as umbral flashes and light bridge flashes (see Thomas 1985, for a comprehensive review). Bogdan & Judge (2006) analyzed the photospheric herring bone pattern and suggested that this pattern is not a physical wave, but apparent motion across the umbra at both photospheric and chromospheric altitudes.

The nature of umbra oscillations has been a subject of debate, and many questions on the physics of umbra waves have been answered. One view is that the oscillations above sunspot umbra are standing acoustic waves (e.g., Georgakilas, Christopoulou, & Koutchmy 2000). This view is based on the idea that the photosphere and the transition region form the walls of a chromospheric resonance cavity and reflect slow magneto-acoustic wave (e.g., Thomas 1985). Through numerical simulation, Botha et al. (2011) demonstrated that the frequencies equal and above the acoustic cutoff frequency resonate inside the chromospheric cavity. They concluded that quasi-monochromatic oscillations in the cavity can be obtained without any clear three-minute source in the photosphere. In that model the chromospheric oscillations leak in the corona, where they form quasi-periodic longitudinal waves propagating at the sound speed along the magnetic field lines (De Moortel & Nakariakov 2012). The other view is that the oscillations are propagating waves moving from photosphere and steeping into shocks in the umbra chromosphere (e.g., Lites 1992). The main criticism against this interpretation is that the source of the oscillations at photospheric level is not well defined. **The need for further advancing of our understanding of sunspot oscillations stimulated a new wave of observational studies with the use of new instrumentation. In particular, Stangalini et al. (2012) reported recently that they found three-minute oscillation in the photospheric part of the umbra, and found out that their amplitude depends on the magnetic field strength. Tian et al. (2014) concluded that the umbra oscillations are upward propagating magneto-acoustic shock waves based**

**on the transient region and chromosphere observations of a sunspot by using Interface Region Imaging Spectrograph (IRIS, De Pontieu et al. 2014).**

It remains a question whether umbra oscillations are connected with running penumbra waves (RPW) or not. Some researchers (e.g., Bloomfield, Lagg, & Solanki 2007) demonstrated that three-minute oscillations in the umbral waves are not the source of RPW. Others insisted that the three-minute oscillations penetrate into the penumbra and propagate further as RPW (Christopoulou, Georgakilas, & Koutchmy 2001). As an evidence supporting their argument, they proposed that the frequency of the oscillation and the propagation velocity of RPW are largest at the inner boundary of the penumbra, and the frequency drops and the speed decreases at the outer penumbra.

Most studies of umbra oscillations have been based on sunspot observations. Pores are patches of a strong magnetic field, only about a few Mm wide at the photosphere. Due to their simple prevailingly vertical structure of the magnetic field without penumbra structures, pores can be exploited to study how umbra oscillations are generated and transported, and interact with ambient magnetic fields in quiet regions. We revisit the study of umbra oscillations by using a high-resolution observation of pores, aiming to understand the nature of the oscillations and their physical properties.

Our study is based on the observation with the Fast Imaging Solar Spectrograph (FISS, Chae et al. 2013) installed on the 1.6-m New Solar telescope (NST, Goode et al. 2010) at the Big Bear Solar Observatory (BBSO). FISS is a unique system that can perform fast-scan spectroscopy of extended areas with dual-spectral measurement of Ca II 8542 Å and H $\alpha$  bands simultaneously. Thanks to the aid of the 308 sub-aperture adaptive optics, we obtained high spatial resolution data of two merged pores by using FISS, which provided raster images with high time (20 seconds), spatial ( $\sim 0.35$  arc second), and spectral (0.019 Å for H $\alpha$  and 0.025 Å for Ca II 8542 Å) resolutions. The main merit of this study is that propagation and interaction of three-minute umbral oscillations generated in the vertical magnetic fields of the small scale pores were investigated by using the high resolution observations. Multi-band spectral imaging, FISS observations are useful for understanding the dynamics of the waves at different heights and horizontal locations in pores. The plan of this paper is as follows: in section 2, we briefly describe the FISS observations and data processing. A detailed description of the intensity and Doppler velocity oscillations in our observations is given in section 3, and our interpretation and discussion on the basic nature of the oscillations are presented in section 4.

## 2. OBSERVATIONS AND ANALYSIS

The target of the present study is a group of pores in NOAA AR11828 near the solar disk center. Our observations were done on 2013 August 24 with the FISS/NST instrument. The observations were aided by the NST adaptive optics (AO) system with 308 sub-apertures to minimize the seeing-induced image motion in the period of time from 16:52 UT to 17:56 UT. FISS scanned the region including the pores as shown in Figure 1(a), which shows a better quality of imaging than the continuum image taken by the Helioseismic and Magnetic Imager (HMI, Schou et al. 2012) onboard the Solar Dynamics Observatory (SDO, Pesnell, Thompson, & Chamberlin 2012) (Figure 1(b)). The pores have the same negative polarity as shown in the magnetogram data in Figure 1(c). Two pores can be identified by the light bridge seen at the off-band ( $-0.7 \text{ \AA}$ ) image of the FISS  $H\alpha$  line and a weak down-flow strip between two pores seen in the line-of-sight SDO/HMI velocity map in Figure 1(d). The line-of-sight velocity in the photosphere deduced from the HMI data suggests that the pores are surrounded by a strong downflow channel and are filled with weak downflows inside them. The velocity pattern in the pores was predicted by numerical simulations (e.g., Steiner et al. 1998) and reported by high resolution observations (e.g., Cho et al. 2010).

FISS mapped the region in the default observational mode in which the scanner moves one step, waits for each camera to take one frame, and then moves to the next step. Each step took 0.15 s and the slit was moved over 130 steps. We obtain raster-scanned spectral images in two spectral lines,  $H\alpha$  and Ca II 8542  $\text{\AA}$  using a single slit and two cameras. The total number of scans recorded during our observations was 192 at each band. The raster cadence was about 20 s and the exposure times were 30 ms for the  $H\alpha$  and 60 ms for Ca II 8542  $\text{\AA}$  bands. The effective pixel size was 0.16 arcsec along and across the slit. The number of pixels along the slit was about 256 so that the field of view was about 40 arcsec in the slit direction. Thus one raster scan covers the field of view of 40 arcsec (in the slit direction) by 20 arcsec (in the scan direction) with spatial resolution of 0.35 arcsec, which is about twice the pixel size. The spectral coverages of the FISS are from  $-4.9 \text{ \AA}$  to  $+4.9 \text{ \AA}$  for  $H\alpha$ , and from  $-5.8 \text{ \AA}$  to  $+6.7 \text{ \AA}$  for Ca II 8542  $\text{\AA}$ , and their spectral resolutions are approximately 0.019  $\text{\AA}$  for  $H\alpha$  and 0.025  $\text{\AA}$  for Ca II 8542  $\text{\AA}$ . We align 192 time-lapsed scan data set of  $H\alpha$  and Ca II 8542  $\text{\AA}$  with sub-pixel accuracy. The orientation and rotation rate of FISS images are corrected by comparing the first image with the data from SDO/AIA, and applying the known rotation rate of FISS. Details of the basic processing including data acquisition, flat fielding, correction, and compression are described by Chae et al. (2013).

Since the intensity level in the spectral line reflects the line formation height, we investigate the spatiotemporal change of the intensity at different wavelengths. Doppler shift measured from the wings to cores of the lines represents the line-of-sight velocity at a differ-

ent altitude of the atmosphere. In this study we choose the lambdameter method to infer the line-of-sight velocity at different heights, since the lambdameter of a line profile provides much information on the velocity and the formation of the line. Our aim is to inspect the spatiotemporal change of intensity and Doppler velocity with heights, which is necessary for understanding of the nature of the oscillations. The intensity at a fixed wavelength changes not only because of intrinsic changes in thermodynamic parameters, but also because of the motion at the line-affecting height of the atmosphere. The latter shifts the line either blueward or redward, and effectively changes the intensity at a given fixed spectral position. This problem is discussed in detail by Stebbins & Goode (1987), Kulander & Jefferies (1966), and Shchukina, Olshevsky & Khomenko (2009). To avoid the cross-talk between the intensity and Doppler velocity, we adopted the lambdameter method (Deubner, Waldschik, & Steffens 1996), which calculate the middle wavelength of fixed width ( $2\Delta\lambda$ ) of a line profile. Using this method we can determine Doppler velocity and the corresponding intensity level independently. More detail procedure of the method is described with illustration at Figure 3 of Chae et al. (2014).

### 3. RESULTS

#### 3.1. General Characteristics of the Pores

Multi-wavelength structures of the pores and their surrounding area can be seen in the FISS  $H\alpha$  and Ca II 8542 Å movies supplied in the electronic version of this journal. The movies contain time-lapse monochromatic images at the far wing ( $-2.0$  Å), blue and red wings ( $0.7$  Å) and the core ( $0.3$  Å) of the spectral lines, as well as line center of the two bands. In both bands, photospheric features are dominant at outer wings, while the line cores and centers gradually sample the chromospheric features. The features seen in  $H\alpha$  and Ca II 8542 Å lines look a little different, which may be due to the difference in the formation heights of the lines. In the monochromatic  $H\alpha$  core and center movies, we notice that the pores are surrounded by thin and long dark structures (fibrils) that emanate from the boundary of pores and are rapidly expanded with the canopy structure. The  $H\alpha$  line is formed either in the chromosphere fibrils or in the deep photosphere whereas the Ca II 8542 Å line samples the layer in between the fibrils and the photosphere. Generally, dark  $H\alpha$  fibrils correspond to higher density structure, and Ca II brightness is more related to temperature (Cauzzi et al. 2008). The formation of  $H\alpha$  line has been investigated in detail by Rutten & Uitenbroek (2012) and references therein.

Time-lapsed images show that the two pores are seen to merge at the beginning of our observations at 16:49 UT in  $H\alpha$ . At the beginning, they could not be easily separated in

the far wing spectra ( $-2.0 \text{ \AA}$ ) of the  $H\alpha$  but there is a faint light bridge between the pores at the near wing spectra ( $-0.7 \text{ \AA}$ ) of the  $H\alpha$  and the continuum spectra ( $-4.0 \text{ \AA}$ ) near the Ca II 8542  $\text{\AA}$  line. The distance between the pores becomes larger after the appearance of a light bridge at 17:15 UT in the far wing spectra ( $-2.0 \text{ \AA}$ ) of the  $H\alpha$ , and their separation can be seen clearly in both bands in the later phase of the observations around 17:56 UT.

The most dynamic features are the sudden brightening observed in the core of the  $H\alpha$  and Ca II 8542  $\text{\AA}$  bands, which corresponds to the well known umbral oscillations (UOs). It looks likely that two pores generate different UOs and their source locations in the pores are changing with time. The UOs emanate and radially expand more or less isotopically from the origin beyond the dark boundary of the pores. Their intensities vary with time and repeat with about every 3 minutes. To inspect the propagation of the UO in the horizontal direction, we have constructed a series of running difference images taken in the  $H\alpha$  and Ca II 8542  $\text{\AA}$  lines as shown in Figure 2. Upper and lower panels show the images from the core ( $-0.3 \text{ \AA}$ ) lines of Ca II 8542  $\text{\AA}$  and  $H\alpha$ , respectively. We have found that the UO expands in the form of arcs and propagates with either circularly or semi-circularly from the center of each pore. The brightest parts are located at the leading edge of the arc at the Eastern and Western sides of the merged pores.

### 3.2. Intensity Oscillations

Figure 3 shows continuum images taken at the  $H\alpha$  (right) and Ca II 8542  $\text{\AA}$  (left) bands with the FISS. The continuum images show the photosphere of the observed region. The region consisted of two pores less than 5 arcsec in diameter and a bright bridge between them. We choose a line along the propagation direction of the UO leading edge and set center positions of the left pore (‘B’), the light bridge (‘C’), and the right pore (‘D’) to inspect intensity and Doppler velocity oscillations at different heights and horizontal locations in the pores, as well as their propagation. We find that most UOs are generated at the positions near ‘B’ and ‘D’. The light bridge is located where two UOs generated at two different pores meet each other. A roughly estimated plane-of-sky speed of the bright leading edge in Figure 2 along the line from ‘B’ to ‘A’ is about  $55 \text{ km s}^{-1}$ . This value is greater than the sound speed (about  $20 \text{ km s}^{-1}$ ) but lower than the Alfvén speed in the chromospheric part of a pore or a sunspot.

Time variation of the features along the line from ‘A’ to ‘E’ can be seen from Figure 4. The propagation of the UOs has been investigated in detail with the time-distance diagram of the intensity perturbations. Upper two panels show the results for the line core ( $-0.3 \text{ \AA}$ ) and the center ( $0.0 \text{ \AA}$ ) of the Ca II 8542  $\text{\AA}$  line. Lower two panels show results for the line

core ( $-0.3 \text{ \AA}$ ) and the center ( $0.0 \text{ \AA}$ ) of the  $H\alpha$  line. The location of the pores' center and the bright bridge between them are denoted by the colored horizontal lines and the boundaries of the pore along the path in Figure 3 are marked by dashed horizontal lines. We can see an inclined strip-like structure with an oscillation pattern in the time-distance intensity maps at the line core and center of  $\text{Ca II } 8542 \text{ \AA}$  and  $H\alpha$ , while the structure cannot be clearly seen in the line-wing intensity maps. While the structures from the core and center of the  $\text{Ca II } 8542 \text{ \AA}$  are similar, strips from the line core of  $H\alpha$  have a higher contrast than those from the  $H\alpha$  line center. The irregular pattern of the strip indicates that UOs propagate more or less isotropically from their origins that are generated at different locations in the pores. There is overlapping of the bright strips coming from the upper part and lower part of the line, which indicates that the UOs coming from the upper and lower parts of the light bridge do not interfere with each other. The apparent propagation speed decreases slowly after the UOs go over the pores' boundary denoted by the white dashed horizontal line in Figure 4. Outside the pores we find a few bright points where two strips merge, but we cannot see any bright features inside the pores where two strips meet, especially near the light bridge.

From the time-distance diagram, we identify that the oscillations at different locations along the line have different phases and periods. It is noticed that there is a short oscillation ( $\sim 3$  minute) in the pores that usually merge into a long period oscillation outside of the pores. This result is consistent with the short-to-long period transition which Chae et al. (2014) noted and attributed to the merging of shocks. We investigate an intensity oscillation at the point 'B' in different bands (Figure 5). The upper panel shows the intensity variations in the  $\text{Ca II } 8542 \text{ \AA}$  band. The lower panel shows the intensity variations in the  $H\alpha$  band. Thick and thin lines indicate the line center and core ( $-0.3 \text{ \AA}$ ) intensities. A sudden drop at 17:32 UT is an artifact due to loss of the data. Through the time lag analysis, we find that the oscillation of the line-core intensity precede the line center by 31 seconds for the  $\text{Ca II } 8542 \text{ \AA}$  band, and 35 seconds for the  $H\alpha$  band, respectively. The oscillations in the  $H\alpha$  band are preceded by the oscillations in the  $\text{Ca II } 8542 \text{ \AA}$  band by 7 seconds and 3 seconds in their core and line intensities, respectively. It is believed that the height of  $H\alpha$  line center formation is higher than that of  $\text{Ca II } 8542 \text{ \AA}$  line center, and cores of  $H\alpha$  and  $\text{Ca II } 8542 \text{ \AA}$  are located below those of line centers. The cross-correlation coefficient of the intensity oscillations between the line center and core of  $H\alpha$ , and that between those of  $\text{Ca II } 8542 \text{ \AA}$  are about 0.7 and 0.5, respectively. These values of the cross-correlation coefficients were archived for the time lags mentioned above. The phase difference between the oscillations seen in different parts of the spectrum supports the idea that the umbral oscillations are an upwardly propagating wave.



### 3.3. Doppler velocity oscillations

To obtain line-of-sight (LOS) velocity maps, we use the smoothed spectrum with a  $0.1 \text{ \AA}$  window from the spectral lines calibrated by adopting two telluric lines of water vapor in the vicinity of each line ( $6561/6565 \text{ \AA}$  for  $H\alpha$ ,  $8541/8546 \text{ \AA}$  for  $\text{Ca II } 8542 \text{ \AA}$ ). Then the lambdameter method was applied to the half line width ( $\Delta\lambda$ ) ranges of  $\Delta\lambda = 0.10 - 0.65 \text{ \AA}$  in  $\text{Ca II } 8542 \text{ \AA}$  and  $H\alpha$ . **The lambdameter method fits a horizontal chord of a pre-defined length into a line profile connecting the blue and red wings. The intensity is then determined at the level where the line width is equal to the chord and the line shift is determined as a difference between the position of the mid-point of the chord and the center of the non-shifted  $H\alpha$  line (See Figure 6).** We performed such measurements using 20 chords of different length  $2\Delta\lambda$ , where  $\Delta\lambda$  ranges from  $0.1 \text{ \AA}$  to  $0.65 \text{ \AA}$ . To improve signal-to-noise ratio, we averaged measurements at every five consecutive chord positions thus obtaining intensity and Doppler shift measurements at four broad ranges along the spectral lines. Before the average, we subtracted the median LOS velocity of each image at a given  $\Delta\lambda$  and time. In this study we use data for only two ranges defined between  $\Delta\lambda=0.1 - 0.21 \text{ \AA}$  and  $\Delta\lambda=0.24 - 0.36 \text{ \AA}$  in the  $\text{Ca II } 8542 \text{ \AA}$  and the  $H\alpha$ ), since oscillation features cannot be clearly seen in the wing spectral signals of both lines. Figure 7 presents time-lapsed Dopplergrams constructed from the near core bandwidth of  $\text{Ca II } 8542 \text{ \AA}$  (upper) and  $H\alpha$  (lower) for a short time period between 16:50:49 UT and 16:52:47 UT. We can see a red-shift spot that expands and propagates outwards from the center of each pore, especially in  $H\alpha$ . The LOS velocity movie obtained from the near core of the  $H\alpha$  and  $\text{Ca II}$  show alternate Doppler shifts that start from the center of pores and then expand in the Eastern and Western directions. They are often seen to propagate far beyond the pores' boundary until they reach the downflow patches associated with the fibrils surrounding the pores. The propagation of the oscillations is clearly seen in the time-distance maps of the Doppler velocity, constructed by using the line cores spectra along the path shown in Figure 3. The upper two panels of Figure 8 are the Doppler maps made for the signals obtained in the near core (a) and far core (b) of the  $\text{Ca II } 8542 \text{ \AA}$  band. The lower two panels show the Doppler maps made for the signals obtained in the near core (c) and far core (d) of the  $H\alpha$  band. In the maps, the red color indicates the plasma moving away from the observer (red-shift), and the blue color indicates the plasma moving towards the observer (blue-shift). In Figure 8, the positions marked in Figure 3 are denoted by the color lines, and the boundaries of the pores are marked by the dashed lines. We can see that in the Doppler shift there is an oscillation pattern which is similar to oscillation detected in the intensity signal (Section 3.2). In the oscillatory signal, there is a sharp change from red to blue, which is more clearly seen in the velocity maps obtained from near-core spectra

of the  $H\alpha$  band. The velocity amplitude from the near-core spectra of  $H\alpha$  is higher than those from far-core spectra of  $H\alpha$ . This effect may be attributed to the density stratification, if the kinetic energy in the wave is conserved and the wave propagates upwards. A weak pattern can be seen in the maps from the core spectra of  $\text{Ca II } 8542 \text{ \AA}$ . We can see that the red strips in Figure 8 start from different locations in the pores and there is no interference between them in the pores. The slope of the strip starts to decline slowly when it meets with the boundary of the pores, which is similar to the pattern of the intensity strips shown in Figure 4. We find that there is suppression of the blueshift when the red strips meet the downflow patches associated with fibrils.

To investigate the relationship between temporal change of intensity and Doppler velocity, we compare the Doppler velocity and the corresponding intensity level independently determined using the lambdameter method. Figure 9 shows the comparison between the intensity and Doppler-shift oscillations at the position ‘B’ (see Figure 3). The upper and lower panels present oscillations of the  $\text{Ca II } 8542 \text{ \AA}$  and  $H\alpha$  estimated from the near-core bandwidth ( $\Delta\lambda = 0.1 - 0.21 \text{ \AA}$ ), respectively. The estimated Doppler velocity ranges from  $-1 \text{ km s}^{-1}$  to  $+4 \text{ km s}^{-1}$  for the  $\text{Ca II } 8542 \text{ \AA}$  and from  $-5 \text{ km s}^{-1}$  to  $+5 \text{ km s}^{-1}$  for  $H\alpha$ . It is noted that the amplitude of the intensity and Doppler velocity perturbations from the  $H\alpha$  core are about two times greater than those from the  $\text{Ca II } 8542 \text{ \AA}$  core. We find no phase difference between the intensity oscillation and Doppler shift oscillation at the core spectra of the  $\text{Ca II } 8542 \text{ \AA}$  and  $H\alpha$ . Such a behavior is typical for propagating slow magnetoacoustic waves (e.g. Verwichte et al. 2010).

#### 4. DISCUSSION AND CONCLUSION

We present our finding on umbral oscillations in the chromospheres of two merged pores observed on 2013 August 24 in AR11828 near the solar disk center. The umbral oscillations are seen as traveling features running from the pores’ centers. To clarify the nature of waves associated with the umbral oscillations, we used the high time, spatial, and spectral resolution data taken by the FISS of the 1.6-meter NST. We infer the line-of-sight velocity by applying the lambdameter method to the high resolution imaging spectrograph data, and investigate the intensity and velocity perturbations at different heights and positions at the pores. Comparing to previous studies of sunspots oscillations, this study is based on the observation of pores, since they provide a relatively simple magnetic field configuration that can be exploited to reveal the nature of magnetoacoustic waves in magnetic fields. Observations of the propagation and interaction of waves in pores atmospheres have rarely been reported in comparison with observations of sunspot dynamics. A similar case was

recently considered by Sobotka et al. (2013), who studied oscillations in a pore in the data of spectral imaging observations in Ca II and complementary spectropolarimetry in Fe I lines. In agreement with our study, concentric running waves originating in the centre of a pore and propagating beyond the pore’s boundary were detected in both Ca II signal intensity and the Doppler shift.

Three-minute intensity and Doppler oscillations were detected in our study inside the pores at the core spectra of Ca II 8542 Å and H $\alpha$ , associated with umbral oscillations. The umbral oscillations were seen to perform a horizontal motion at the speed about 55 km s<sup>−1</sup>, that is faster than the sound speed but slower than the Alfvén speed in the chromosphere. The propagation speed was found to decrease slowly and the periods increase after the umbral oscillations travel over the boundary of the pores. The measured value of the horizontal speed is different than about 9 km s<sup>−1</sup> measured by Sobotka et al. (2013).

Our findings support the interpretation of the umbral oscillations in terms of upwardly propagating slow magnetoacoustic waves. **In the low- $\beta$  plasma of the sunspots chromosphere, this mode propagates mainly along the magnetic field at the speed about the sound speed, and is essentially compressive.** In this interpretation, the apparent horizontal motion directed from the pores’ centres to their boundaries is associated with the projection of the wave fronts on the horizontal direction, rather than with the true propagation of compressive perturbations across the magnetic field. First, there is a phase difference between the perturbations of the intensities from the near-cores and line centers of Ca II 8542 Å and H $\alpha$ . Time-lag analysis reveals that the line core intensity perturbation precedes the signal in the line center, and H $\alpha$  oscillations are preceded by Ca II 8542 Å oscillations in their core and line center intensity perturbations. Taking that the H $\alpha$  signal is formed higher than the Ca II signal, such a phase difference indicates that the observed oscillating feature is an upwardly propagating wave. Second, our observation shows that the amplitude of the LOS speed determined from the near-core spectra is greater than that estimated from the far-core spectra. The increase in the amplitude from the far- to near-cores can be explained by conservation of kinetic energy in a wave propagating upward in a stratified medium. The decrease in the equilibrium density with height causes the increase in the velocity perturbations in the wave. **Lastly, we found no phase difference between intensity fluctuation and velocity fluctuation. This is a non-trivial finding since the chromosphere is gravitationally stratified and the plasma there may be radiatively cooling. In an adiabatic stratified medium, only the fluctuations with frequencies much higher than the acoustic cutoff frequency can be treated like pure acoustic waves propagating with intensity and velocity oscillating in phase, while intensity fluctuation and velocity fluctuation of frequencies close to or below the cutoff frequency are out of phase with each other with the phase**

difference being about  $90^\circ$  (e.g., Mein 1977). The observed in-phase behavior thus suggests that the local acoustic cutoff frequency should be much lower than the one corresponding to three minutes. This may be because the atmospheric levels seen through the cores of the two lines are higher and much hotter than the temperature minimum. It is also noted that the radiative loss can bring about a significant phase difference between intensity and velocity by smoothing temperature fluctuations (Noyes & Leighton 1963). Our observation, however, suggests that the radiative loss little affects waves, justifying the adiabatic assumption. This may be attributed to the long radiative relaxation time of the chromosphere (Carlsson & Stein 2002).

Based on the above results, we conclude that the apparently horizontally-propagating features (umbral oscillations) detected in the pore atmosphere are a visual pattern of slow magnetoacoustic wave propagating at the local sound speed along the magnetic field. The visual pattern found in the pores is consistent with that of sunspots reported by Bogdan & Judge (2006). This mechanism is illustrated in Figure 10. The dashed curves indicate the wave fronts with the alternate field-aligned compressive flows caused by an upwardly propagating slow wave. Our conclusion from the pores observation is quite consistent with those from the sunspot observations. For example, Centeno et al. (2009) presented that chromospheric oscillation power comes from the photosphere by means of field-aligned wave propagation. The propagation of slow magnetoacoustic mode from the photosphere to the chromosphere was reported from multi-line observations (e.g., Reznikova & Shibasaki 2012; Sych & Nakariakov 2014) and numerical simulations (e.g., Felipe, Khomenko, & Collados 2011). In particular, Bloomfield, Lagg, & Solanki (2007) concluded that running penumbra waves are visible patterns caused by slow-mode waves propagating along the magnetic field in sunspots. In the equilibrium plasma configuration, the magnetic field lines experience the growing inclination from the vertical direction with the increase in the horizontal distance from the pore center. Assuming for clarity that the wave fronts are locally perpendicular to the magnetic field lines, we see that the horizontal level corresponding to the Ca II 8542 Å line formation height, experiencing simultaneously different phases of the slow wave. This causes an apparent horizontal motion of the slow wave phase, e.g., the maximum perturbation of the intensity perturbation, along the horizontal plane of the line formation height. The observed apparent speed of the horizontal motion of the wave phase does not represent any energy or information transfer in the horizontal direction. Moreover, the observed decrease in the phase speed beyond the pore boundary may be explained by the slow wave propagation along the inclined field lines that form the canopy structure. We speculate that the fast traveling feature inside the pores and slow traveling feature outside of the pores are different manifestations of the same phenomenon. In addition, the discrepancy between the values of

the horizontal speeds in Sobotka et al. (2013) and in our study can be readily attributed to the different angles between the LOS, wave front planes and the magnetic fields.

Another interesting finding is that the waves coming from different pores separated by the light bridge do not interfere with each other inside the pores, while the waves escaping the pores’ boundary merge with other waves or surrounding fibrils. The merged flows form single continuous flows, which are observationally identified by the merging of the red-shift ridge and suppression of blue-shift seen in Figure 8. This is quite consistent with the “merging of redshift ridges” or the “fork-pattern of redshift ridges” first clearly pointed out by Chae et al. (2014). They interpret this pattern as the manifestation of the merging of two successive shocks. Note that these patterns were seen in other observations such as Maurya et al. (2013) and Tian et al. (2014). Some of the brightening seen in Figure 4 may be related to the wave coupling or wave-fibril interaction. Our observation shows that waves in two pores are not correlated with each other. It is suggestive of the excitation mechanism of waves in pores. A more extended investigation is required to draw conclusion on the interactions of the waves inside and outside of pores.

We are grateful to the referee for helpful and constructive comments and suggestions. This work was supported by the “Development of Korea Space Weather Center” of KASI and the KASI basic research funds and by the Korea Research Foundation of Korean (KRF-2012R1A2A1A03670387); the European Research Council under the SeismoSun project No. 321141, STFC consolidated grant ST/L000733/1, and the BK21 plus program through the National Research Foundation funded by the Ministry of Education of Korea (VMN).

## REFERENCES

- Beckers, J. M., & Tallant, P. E. 1969, *Sol. Phys.*, 7, 351
- Bhatnagar A., Livingstone W. C., Harvey J. W. 1972, *Sol. Phys.*, 27, 80
- Bloomfield, D. S., Lagg, A., & Solanki, S. K. 2007, *ApJ*, 671, 1005
- Botha, G. J. J., Arber, T. D., Nakariakov, V. M., & Zhugzhda, Y. D. 2011, *ApJ*, 728, 84  
(Bogdan & Judge 2006)
- Bogdan, T.J., & Judge, P. G. 2006, *Royal Society of London Philosophical Transactions Series A*, 364, 313
- Carlsson, M., & Stein, R. F. 2002, *ApJ*, 572, 626

- Cauzzi, G., Reardon, K., Uitenbroek, H., et al. 2008, *A&A*, 480, 515
- Centeno et al. (2009)
- Centeno, R., Collados, M., & Bueno, J. T. 2009, *ApJ*, 692, 1211
- Chae, J., Park, H. M., Ahn, K., et al. 2013, *Sol. Phys.*, 288, 1
- Chae, J., Yang, H., Park, H., et al. 2014, *ApJ*, 789, 108
- Cho, K.-S., Bong, S.-C., Chae, J., Kim, Y.-H., Park, Y.-D. 2010, *ApJ*, 723, 440.
- Cho, K.-S., Bong, S.-C., Chae, J., et al. 2013, *Sol. Phys.*, 288, 23.
- Christopoulou, E. B., Georgakilas, A. A. & Koutchmy, S. 2001, *A&A*, 375, 617
- de la Cruz Rodrí, Rouppe van der Voort, L., Socas-Navarro, H., & van Noort, M. 2013, *A&A*, 556, A115
- De Moortel, I., & Nakariakov, V. M. 2012, *Royal Society of London Philosophical Transactions Series A*, 370, 3193
- De Pontieu, B. et al. 2014, *Sol. Phys.*, 289, 2733
- Deubner, F.-L., Waldschik, T., Steffens, S. 1996, *A&A*, 307, 936
- Felipe, T., Khomenko, E., & Collados, M. 2011, *ApJ*, 735, 65
- Georgakilas, A. A., Christopoulou, E. B., & Koutchmy, S. 2000, *A&A*, 363, 306
- Giovanelli, R. G. 1972, *Sol. Phys.*, 27, 71
- Goode, P. R., Coulter, R., Gorceix, N., Yurchyshyn, V., & Cao, W. 2010, *Astron. Nachr.*, 331, 620
- Kulander, J. L., & Jefferies, J. T. 1966, *ApJ*, 146, 194
- Lites, B. W. 1992, in *NATO ASIC Proc. 375: Sunspots. Theory and Observations*, 261
- Mein, N. 1977, *Sol. Phys.*, 52, 283
- Martinez Pillet, V., Lites, B. W., & Skumanich, A. 1997, *ApJ*, 474, 810
- Maurya, R. A., Chae, J., Park, H., et al. 2013, *Sol. Phys.*, 288, 73
- Noyes, R. W., & Leighton, R. B. 1963, *ApJ*, 138, 631

- Pesnell, W. D., Thompson, B.T., & Chamberlin, P.C. 2012, *Sol. Phys.*, 275, 3
- Reznikova, V. E. & Shibasaki, K. 2012, *ApJ*, 756, 35
- Roupper van der Voort, L. H. M., Rutten, R. J., Sütterlin, P., Sloover, P. J., & Krijger, J. M. 2003, *A&A*, 403, 277
- Rutten, R. J. & Uitenbroek, H. 2012, *A&A*, 540, A86
- Schou, J., Scherrer, P. H., Bush, R. I. et al. 2012, *Sol. Phys.*, 275, 229
- Shchukina, N. G., Olshevsky, V. L., & Khomenko, E. V. 2009, *A&A*, 506, 1393
- Sobotka, M., Švanda, M., Jurčák, J., et al. 2013, *A&A*, 560, A84
- Stangalini, M., Giannattasio, F., Del Moro, D., & Berrilli, F. 2012, *A&A*, 539, L4
- Stebbins, R., & Goode, P. R. 1987, *Sol. Phys.*, 110, 237
- Steiner, O., Grossmann-Doerth, U., Knoelker, M., & Schuessler, M. 1998, *ApJ*, 495, 468
- Sych, R., & Nakariakov, V. M. 2014, *A&A*, 569, A72
- Thomas, J. H. 1985, *Australian Journal of Physics*, 38, 811
- Tian, H. et al. 2014, *ApJ*, 786, 137
- Tziotziou, K., Tsiropoula, G., Meun, N., & Mein, P. 2006, *A&A*, 456, 689
- Verwichte, E., Marsh, M., Foullon, C., et al. 2010, *ApJ*, 724, L194
- Zirin, H. & Stein, A. 1972, *ApJ*, 178, L85

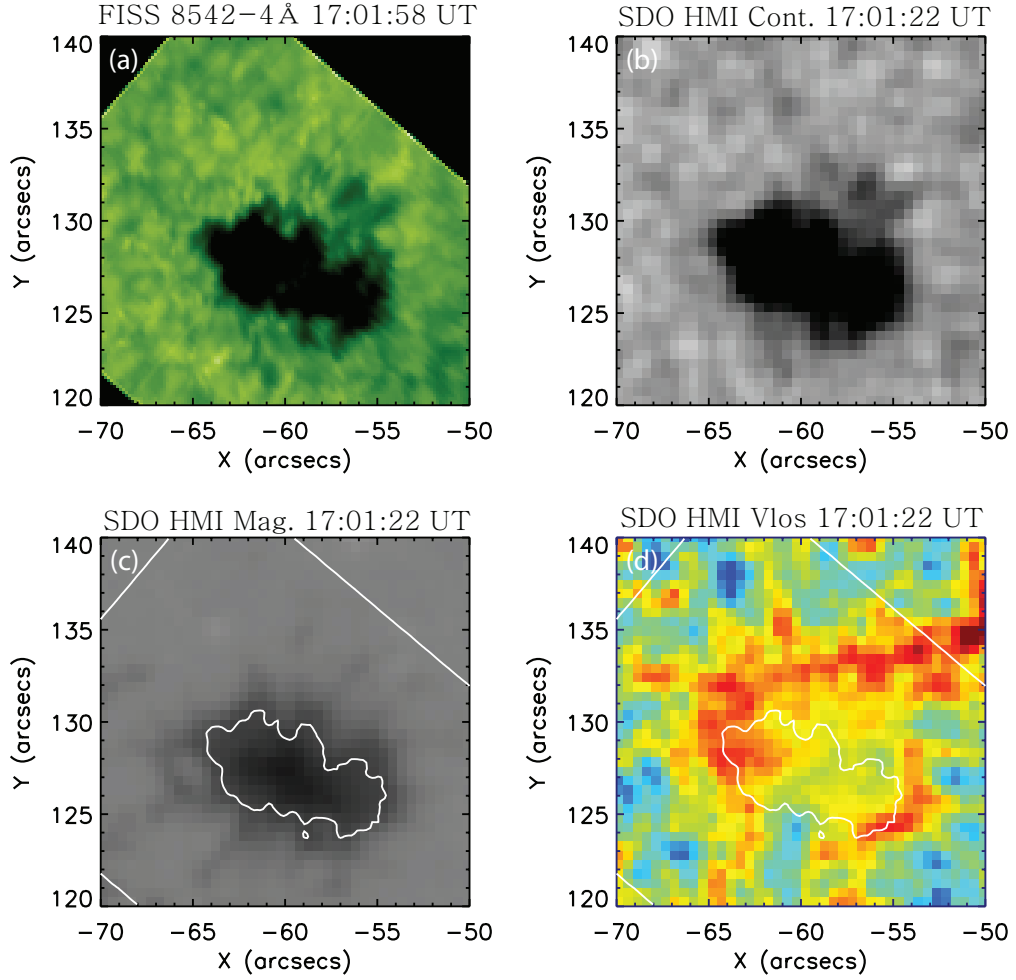


Fig. 1.— Two merged pores in an active region (AR11828) observed by the NST/FISS and the SDO/HMI. The upper left panel is the FISS continuum image at Ca II 8542 Å taken at 17:02 UT on August 24, 2013. The upper right panel is the HMI continuum image of the solar photosphere, while lower panels show HMI line-of-sight magnetic field (left) and HMI Doppler velocity (right) maps.



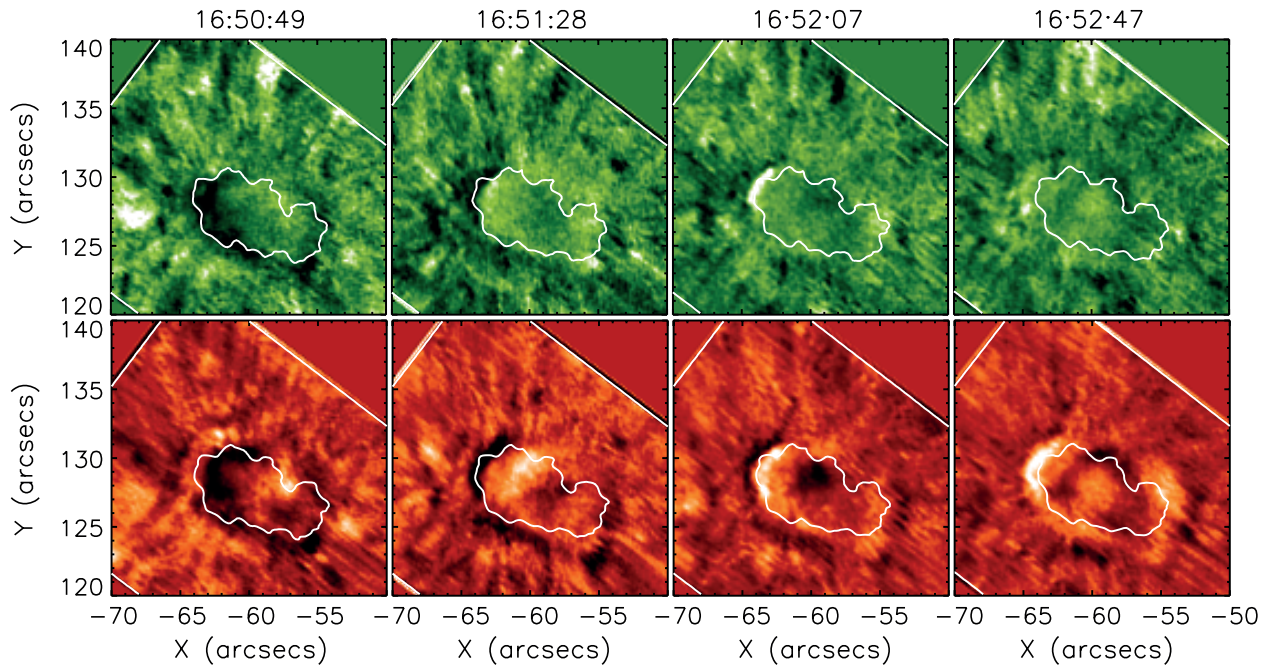


Fig. 2.— Running difference images of Ca II 8542 Å line core ( $-0.3$  Å, upper panels) and H $\alpha$  line core ( $-0.3$  Å, lower panels), showing traveling features (UO). The white contour marks the boundary of the pore.

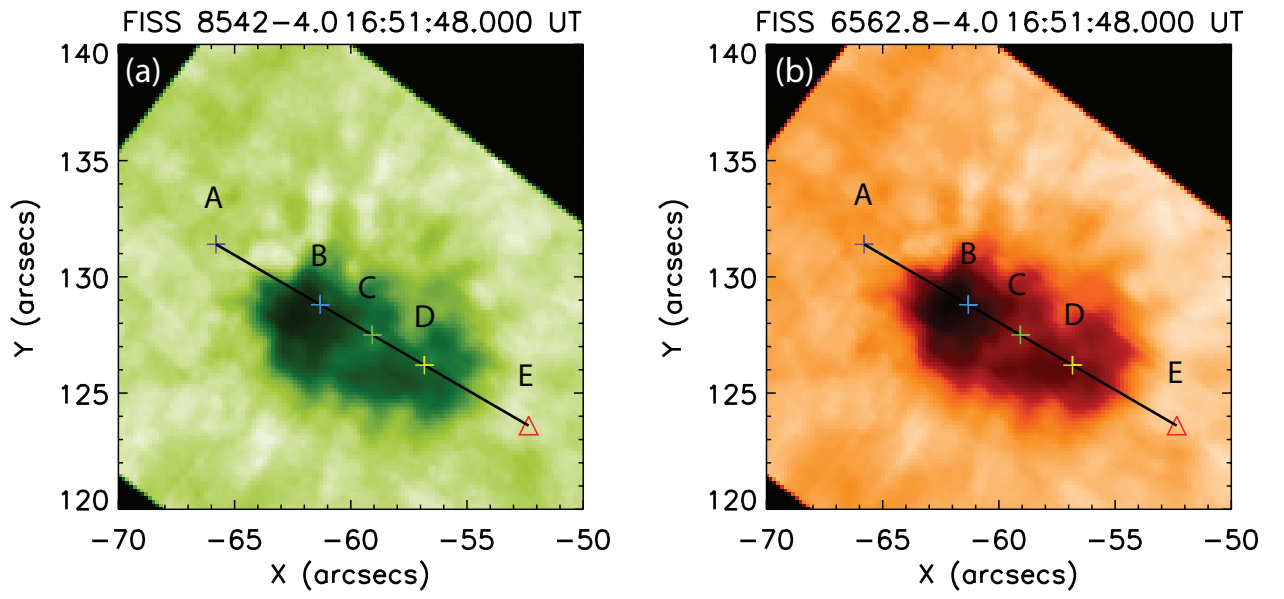


Fig. 3.— Continuum images at Ca II 8542 Å line wing (a, -4.0 Å) and H $\alpha$  line wing (b, -4.0 Å). A path for tracking the traveling features is denoted by the black line and the locations for inspection of intensity and Doppler speed oscillations are labeled by ‘A’ – ‘E’.

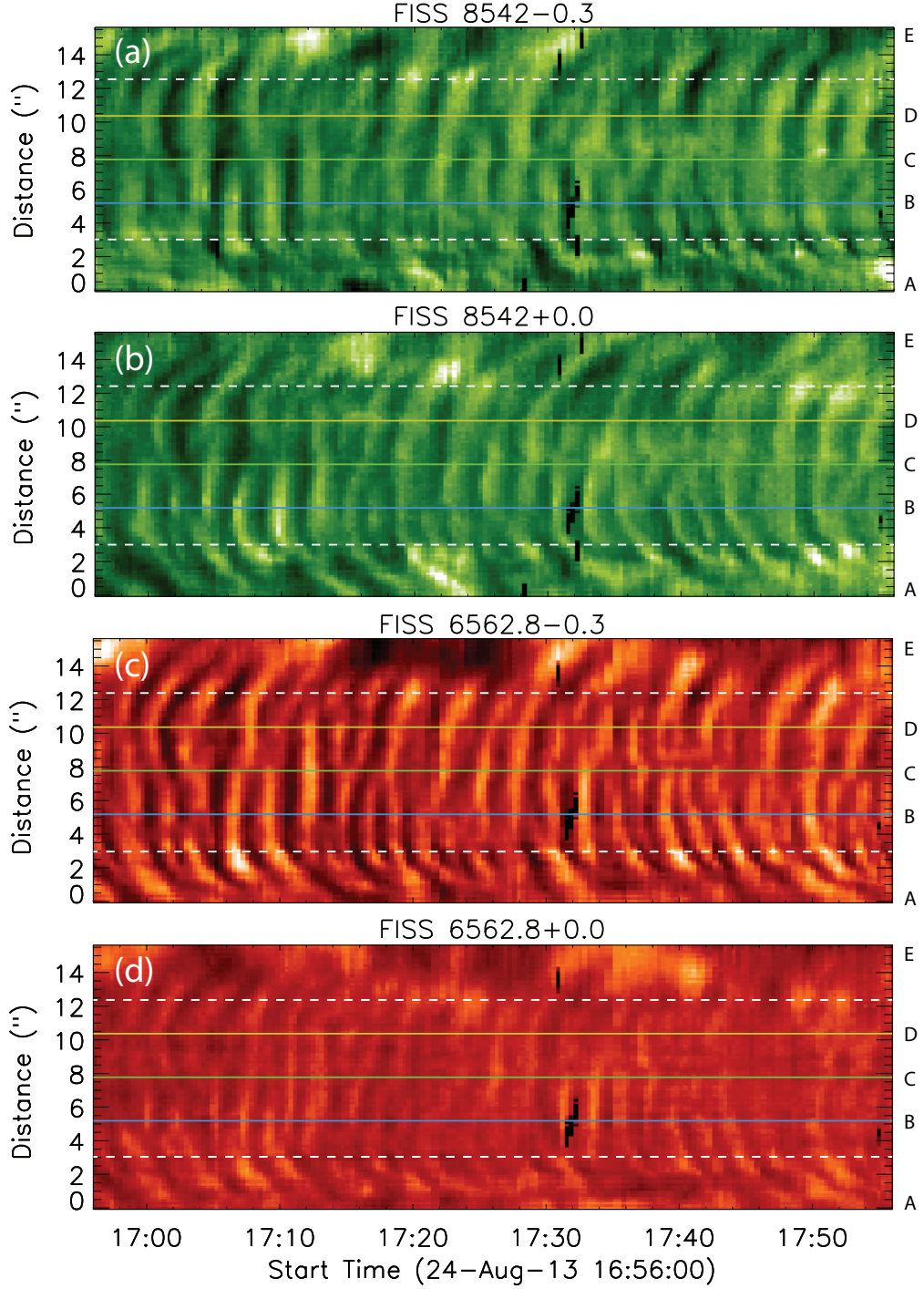


Fig. 4.— Time-distance maps of the Ca II 8542 Å band (upper two panels) and H $\alpha$  band (lower two panels) along the path in Figure 3. The horizontal axis represents time and the vertical axis represents the position along the path. The colored solid lines denote the locations marked with symbols in Figure 3, and the dotted lines represent the boundary of the pore.

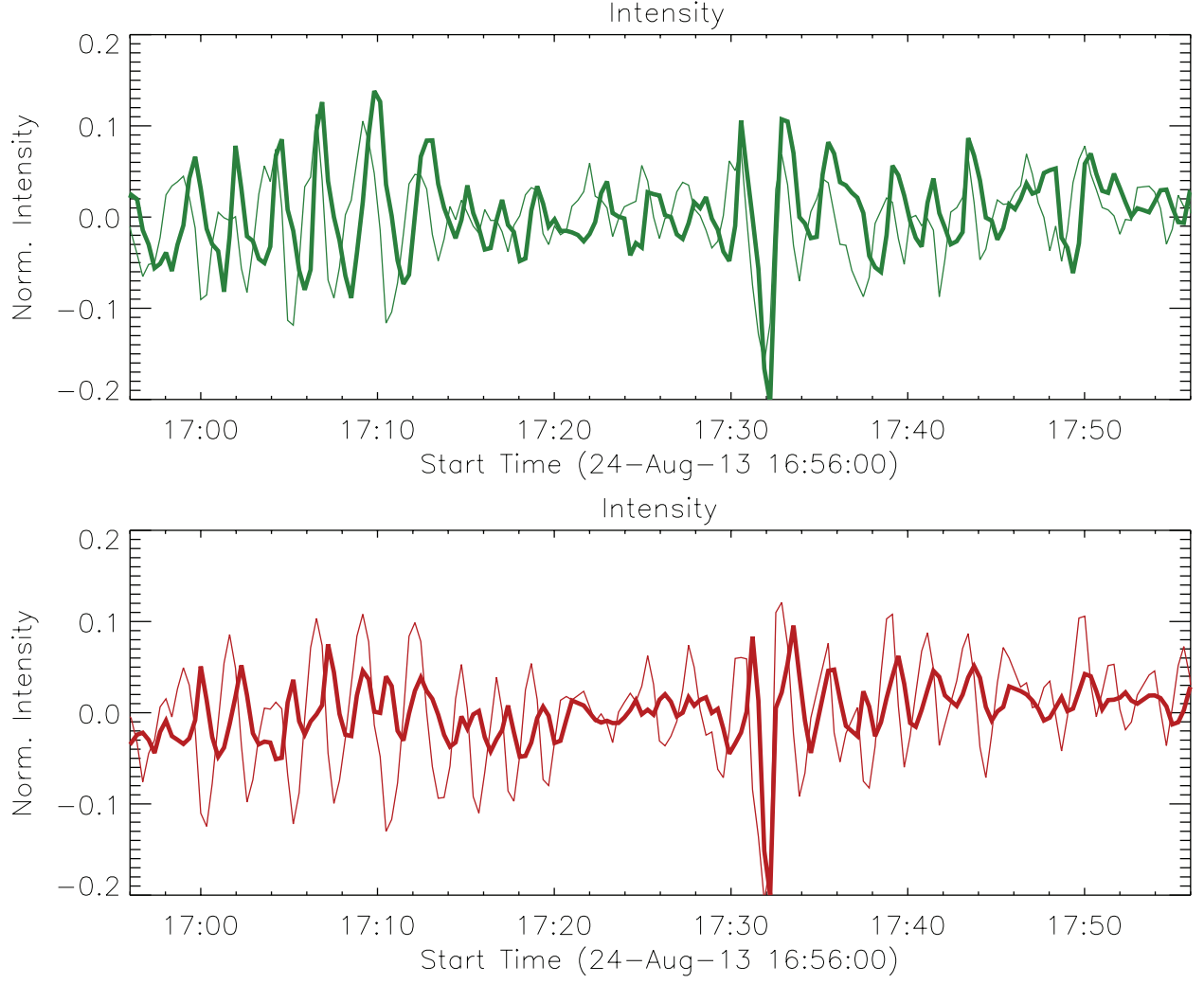


Fig. 5.— Variations of the line core and center intensities for Ca II 8542 Å (upper panel) and H $\alpha$  (lower panel) bands at the position of 'B' in Figure 3 . Thick lines represent the line centers of the bands and thin lines represent the line cores ( $-0.3$  Å from the line center) of the bands.

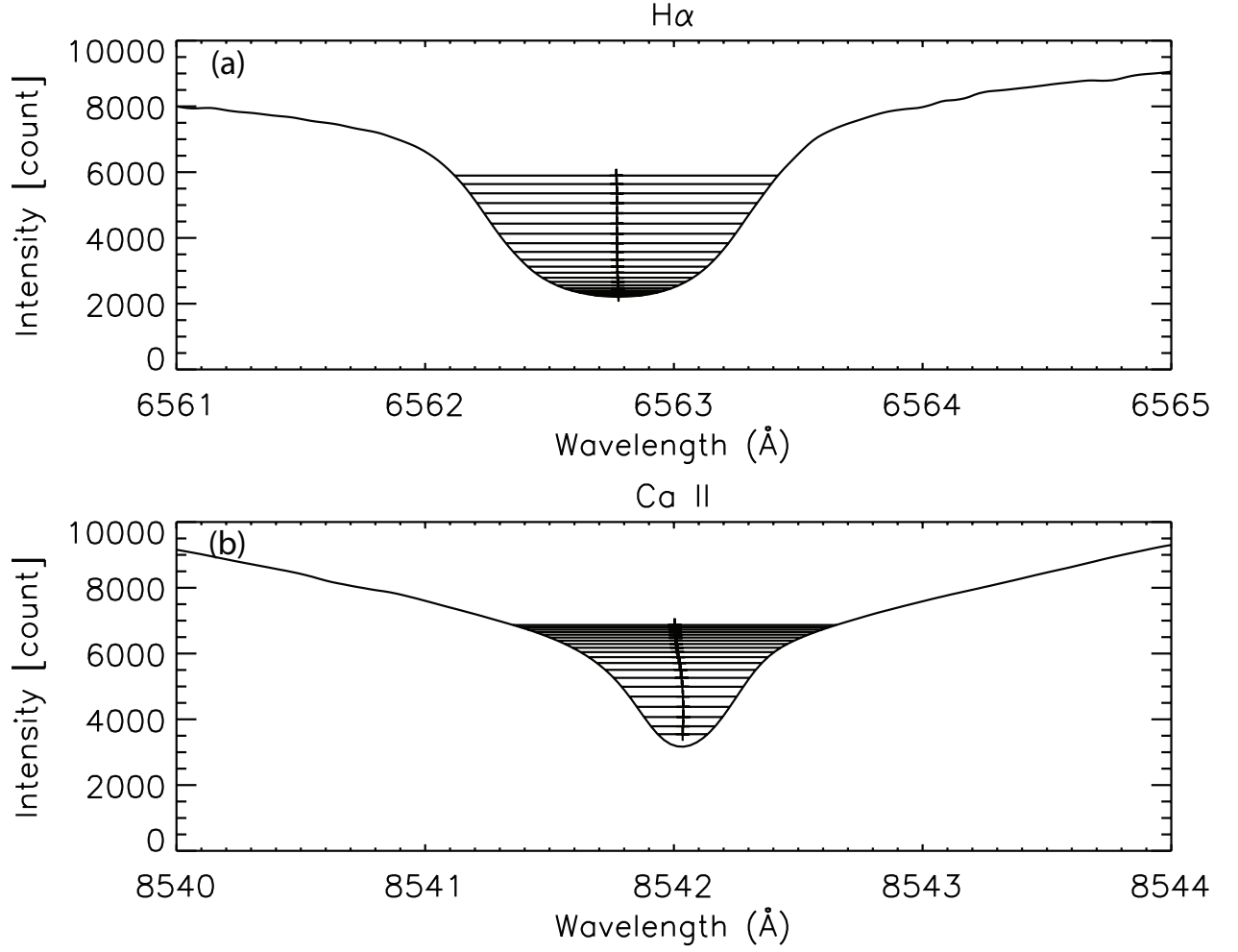


Fig. 6.— FISS H $\alpha$  (upper panel) and CaII 8542 Å (lower panel) lines profiles averaged over FISS FOV. Horizontal line indicates a chord of a pre-defined length fit into the line profile, and plus symbol denotes the position of the mid-point of the chord.

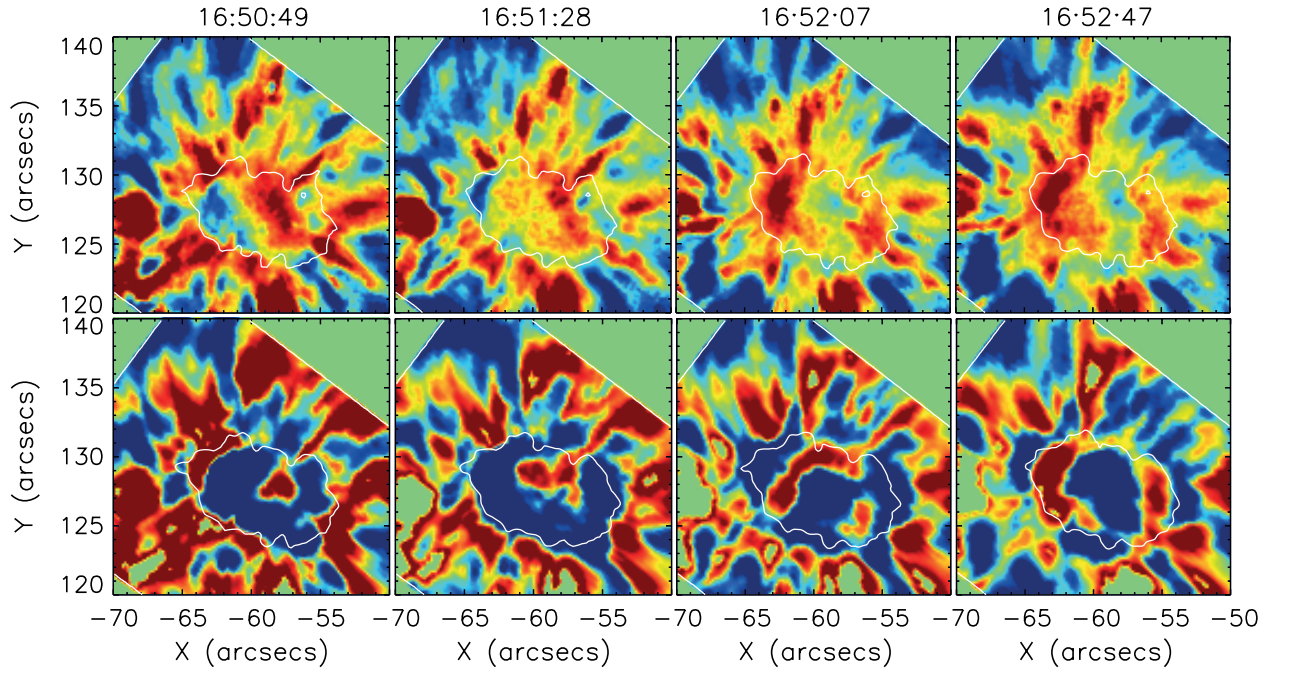


Fig. 7.— Doppler velocity maps constructed by applying the lambdameter method to the line cores of the Ca II 8542 Å ( $\Delta\lambda = 0.1 - 0.21\text{\AA}$ , upper panels) and H $\alpha$  ( $\Delta\lambda = 0.1 - 0.21\text{\AA}$ , lower panels). The red color indicates plasma moving away from the observer (red-shift) and the blue indicates moving toward (blue-shift).



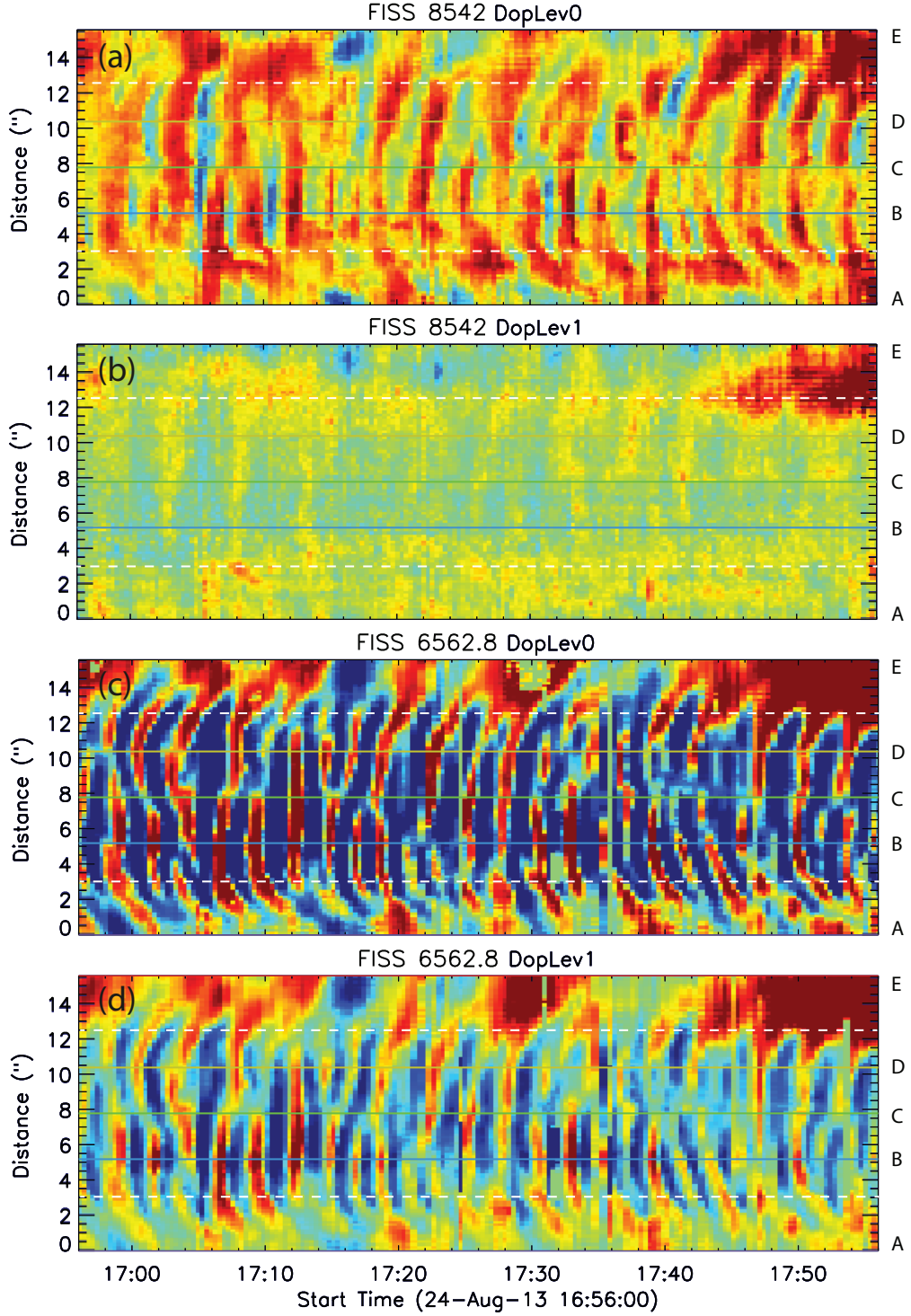


Fig. 8.— Time-distance maps of Doppler velocity constructed along the path in Figure 3. The maps are constructed by using near core (a,  $\Delta\lambda = 0.1 - 0.21\text{\AA}$ ) and far core (b,  $\Delta\lambda = 0.24 - 0.36\text{\AA}$ ) bands of CaII 8542 Å line and H $\alpha$  line. The horizontal and vertical axes, colored solid line, and dotted line represent the same as those in Figure 4.

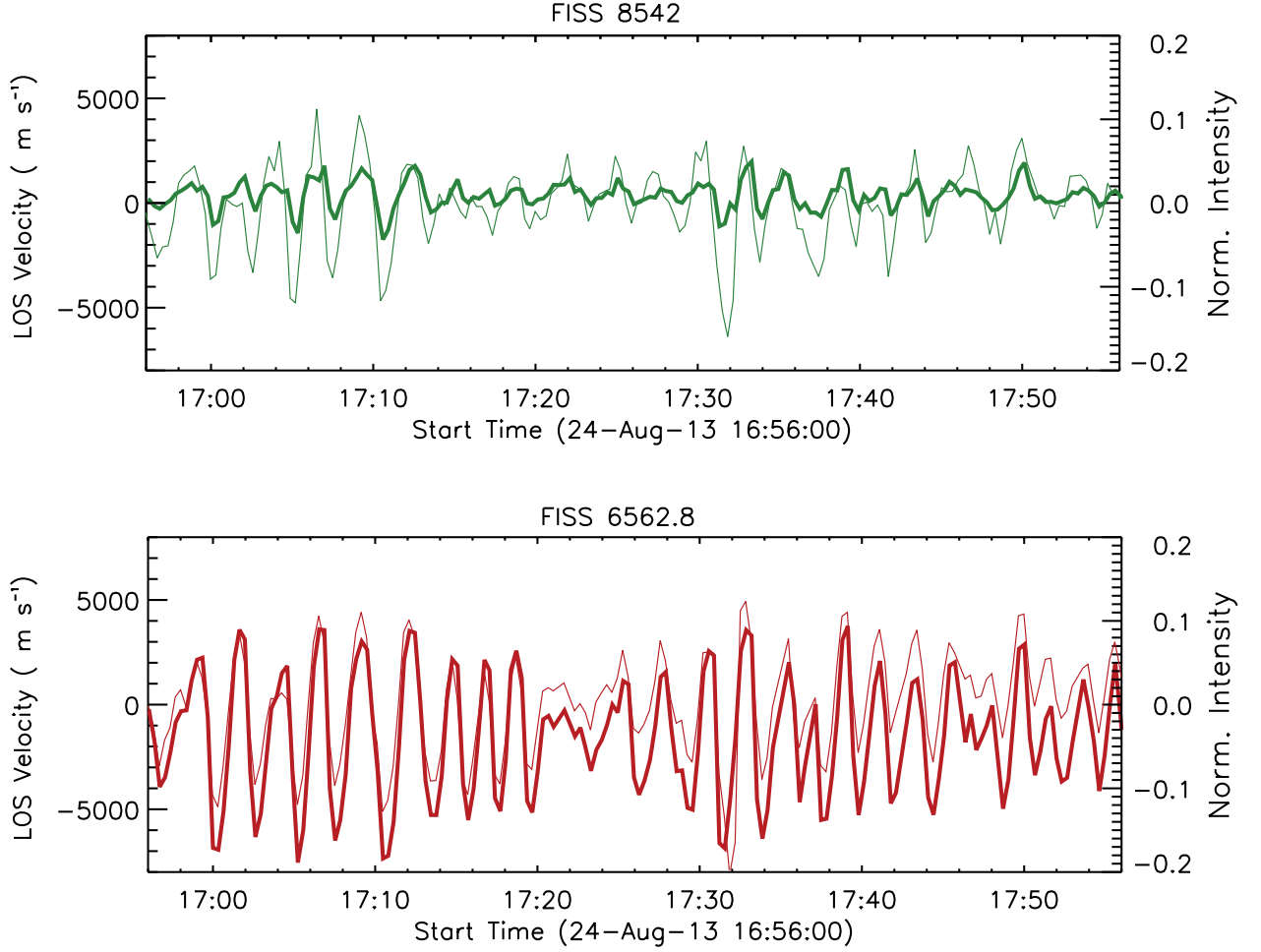


Fig. 9.— Change of intensities and Doppler velocity at Ca II 8542 Å near core ( $-0.15\text{\AA}$ ,  $\Delta\lambda = 0.1 - 0.21\text{\AA}$ ; upper panel) and H $\alpha$  near core ( $-0.15\text{\AA}$ ,  $\Delta\lambda = 0.1 - 0.21\text{\AA}$ ; lower panel) at the position of ‘B’ in Figure 3. Thick and thin lines represent the Doppler velocities and intensity, respectively. Positive value of the Doppler speed indicates a plasma moving away (red-shift) from the observer and negative value indicates moving toward (blue-shift) the observer.



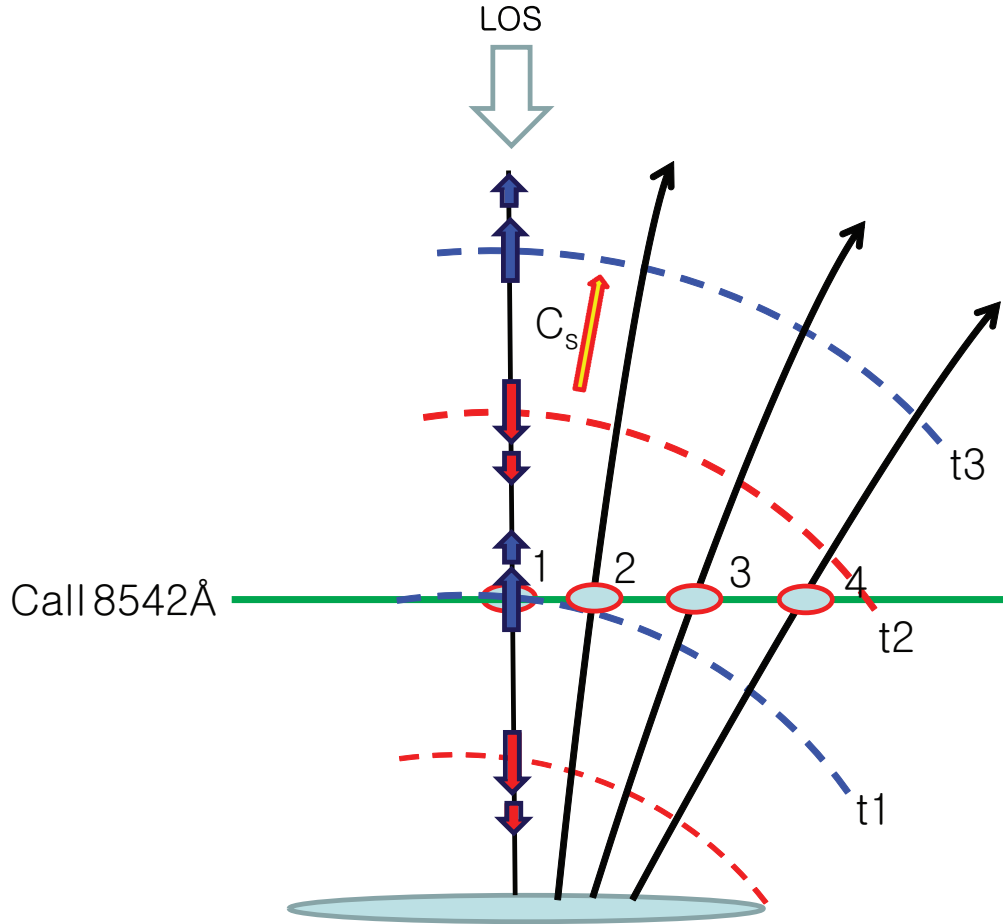


Fig. 10.— A cartoon showing the wave propagation and Doppler velocity change along the magnetic field lines in the pore atmosphere. Black lines represent the magnetic fields and the colored curved lines represent the wave front with downward (red-shift) and upward (blue-shift) moving plasmas.